scientific reports

OPEN

Personalized prediction of gait freezing using dynamic mode decomposition

Zhiwen Fu[1,3], Congping Lin[2,3] & Yiwei Zhang[1✉]

Freezing of gait (FoG) is a common severe gait disorder in patients with advanced Parkinson's disease. The ability to predict the onset of FoG episodes early on allows for timely intervention, which is essential for improving the life quality of patients. Machine learning and deep learning, the current methods, face real-time diagnosis challenges due to comprehensive data processing requirements. Their "black box" nature makes interpreting features and classification boundaries difficult. In this manuscript, we explored a dynamic mode decomposition (DMD)-based approach together with optimal delay embedding time to reconstruct and predict the time evolution of acceleration signals, and introduced a triple index based on DMD to predict and classify FoG. Our predictive analysis shows 86.5% accuracy in classification, and an early prediction ratio of 81.97% with an average early prediction time of 6.13 s. This DMD-based approach has the potential for real-time patient-specific FoG prediction.

Keywords Freezing of gait, Personalized prediction, Dynamic mode decomposition, Triple index

Parkinson's disease (PD) is a prevalent neurological disorder characterized by progressive degeneration of dopaminergic and other subcortical neurons[1]. Besides a flexed posture, tremor at rest, rigidity, akinesia (bradykinesia) and postural instability, motor blocks (i.e., complete inability to move) which most commonly affect the patients' legs during walking, are common negative effects of PD. Freezing of motor blocks (also known as freezing of gait, FoG) is one particularly challenging aspect of PD. It typically manifests as a sudden and transient inability to initiate the next step, and becomes increasingly common as PD progresses[2]. Freezes typically last only a few seconds, up to one minute[3,4], and can lead to falls[5]. Multiple occurrences of FoG throughout a day, not only cause persistent physical risk but also reduce overall quality of life for those who are affected[6].

Early prediction of FoG attacks before they occur[7], allows for timely intervention before the event to prevent the freeze from occurring[8]. Wearable sensors have been used to detect and predict FoG with the ultimate aim of preventing freezes and reducing their effects using gait monitoring and assistive devices. Such wearable sensors are vital for FoG detection and prediction; see reviews e.g.[9,10] and references therein.

Compared to FoG detection, studies of FoG prediction are relatively few[11]. Most of the previous studies focus on the construction of selected time-frequency features and the use of machine learning technology[11–14] to identify the pre-FoG stage, and also utilizing deep learning[11,15–17] for PD diagnosis and classification. While deep learning has demonstrated improved accuracy in diagnosing PD over traditional machine learning algorithms, it currently cannot accurately diagnose and classify PD in real time, as these models tend to be computationally expensive and require large amounts of processing power[11,15,18,19]. Another limitation of current deep-learning-based FoG prediction approaches is that due to the black box property of the deep neural network, the learned feature maps and the classification boundaries are hard to interpret[11].

A popular alternative to machine learning and deep learning is dynamic mode decomposition (DMD)[20,21], which directly approximates the system dynamics observed from time series. DMD provides an appealingly simple yet powerful tool for inferring a local model near steady states and extracting features of inherent dynamic systems from data, thus providing greater flexibility and accuracy in dealing with nonlinear and high-dimensional real-time data[21–23]. So far, DMD has been used for the characterization and quantification of underlying physical mechanisms as well as for the prediction of future system states in various fields, such as fluid flow[24], power systems[25], wind farm control[26], and influenza epidemics[27].

[1]Department of Mathematics and SUSTech International Center for Mathematics, Southern University of Science and Technology, Shenzhen, China. [2]School of Mathematics and Statistics, Hubei Key Lab of Engineering Modelling and Scientific, Center for Mathematical Sciences, Huazhong University of Science and Technology, Wuhan, China. [3]Z. Fu and C. Lin have contributed equally to this work. ✉email: zhangyw@sustech.edu.cn

In this manuscript, we explore a DMD-based approach to understand the inherent dynamic difference between normal and abnormal gaits. If a segment of time series data can be accurately reconstructed by DMD, then the underlying dynamics can be captured and analyzed through the DMD triple. To facilitate the classification of gaits, we introduce a DMD triple index to distinguish between normal and abnormal gaits. Furthermore, from the time evolution of the DMD triple index, we are able to predict the onset of FoG early on using patient-dependent thresholds of the triple index.

Dynamic mode decomposition

In this section, we present the theory of dynamic mode decomposition[22,28] together with delay embedding[29] that approximates the underlying dynamics of time series as a linear system.

Assume that the data $\{x_0, x_1, \ldots, x_n\}$ are equally spaced in time from $t = 0$ to $t = n$, where each $x_i \in \mathbb{C}^m$ is a $m-$dimensional complex vector. Arrange the data into two matrices

$$X_0 := [\ x_0 \quad x_1 \quad \cdots \quad x_{n-1}\ ] \in \mathbb{C}^{m \times n},$$
$$X_1 := [\ x_1 \quad x_2 \quad \cdots \quad x_n\ ] \in \mathbb{C}^{m \times n}.$$

and postulate that the data have been generated by a discrete-time linear time-invariant system $x_{t+1} = Ax_t, t = 0, 1, \ldots, n-1$, i.e, $X_1 = AX_0$.

The economic-size Singular Value Decomposition(SVD) of X_0 reads as

$$\underset{m \times n}{X_0} = \underset{m \times r}{U} \cdot \underset{r \times r}{\Sigma} \cdot \underset{r \times n}{V^*}$$

where r is the rank of the matrix X_0. The standard DMD algorithm provides an optimal representation matrix $K \in \mathbb{C}^{r \times r}$ of the matrix A on the basis spanned by the proper orthogonal decomposition modes of X_0, i.e., $A \approx UKU^*$. The optimal matrix K reads as $K = U^*X_1V\Sigma^{-1}$ which minimizes the Frobenius norm of the difference between X_1 and AX_0 with $A = UKU^*$ and $X_0 = U\Sigma V^*$.

Thus, the dynamics in the r-dimensional subspace is determined by the matrix K, i.e., $y_{t+1} = Ky_t$, $y_t \in \mathbb{C}^r$.

If K has a full set of linearly independent unit-length eigenvectors $\{z_1, \ldots, z_r\}$, with corresponding eigenvalues $\mu_1, \ldots, \mu_r$, then it can be decomposed into a diagonal coordinate form:

$$K = [z_1, \ldots, z_r] \begin{bmatrix} \mu_1 & 0 & 0 \\ 0 & \ddots & 0 \\ 0 & 0 & \mu_r \end{bmatrix} \begin{bmatrix} w_1^* \\ \vdots \\ w_r^* \end{bmatrix} := ZD_\mu W^*,$$

where w_i are eigenvectors of K^* with corresponding eigenvalues $\bar{\mu}_i$ and scaled so that $w_i^* z_j = \delta_{ij}$. Here, an asterisk denotes the complex-conjugate-transpose of a vector (matrix). Thus, the time evolution $y_t = ZD_\mu^t W^* y_0 = \sum_{i=1}^r z_i \mu_i^t w_i^* y_0$.

The matrix U can map y_t to a higher dimensional space $\mathbb{C}^m$ via $x_t \approx Uy_t$. Denote the amplitude $\alpha_i = w_i^* y_0$, DMD modes $\phi_i = Uz_i$ and spectrum $s_i = \ln \mu_i$. Then we have the time evolution

$$x_t \approx Uy_t = \sum_{i=1}^r Uz_i \mu_i^t w_i^* y_0 = \sum_{i=1}^r \alpha_i \phi_i e^{s_i t}, \quad t \in \{0, \ldots, r-1\} \tag{1}$$

or in matrix form

$$\overbrace{[x_0, \ x_1, \ \ldots, x_{n-1}]}^{X_0} \approx \overbrace{[\phi_1, \ \phi_2, \cdots \phi_r]}^{\Phi} \overbrace{\begin{bmatrix} \alpha_1 & 0 & 0 & 0 \\ 0 & \alpha_2 & 0 & 0 \\ 0 & 0 & \ddots & 0 \\ 0 & 0 & 0 & \alpha_r \end{bmatrix}}^{D_a := diag\{\alpha\}} \overbrace{\begin{bmatrix} 1 & e^{s_1} & \cdots & e^{s_1(n-1)} \\ 1 & e^{s_2} & \cdots & e^{s_2(n-1)} \\ \vdots & \vdots & \ddots & \vdots \\ 1 & e^{s_r} & \cdots & e^{s_r(n-1)} \end{bmatrix}}^{V_{\text{and}}}. \tag{2}$$

While minimizing $\|X_0 - \Phi D_\alpha V\|_F^2$ in the Frobenius norm, the optimal amplitude $\alpha := [\alpha_1 \ \cdots \ \alpha_r]^T$ reads as[28]

$$\alpha_{\text{dmd}} = \left((Z^* Z) \circ \overline{\left(V_{\text{and}} V_{\text{and}}^* \right)} \right)^{-1} \overline{\text{diag} \left(V_{\text{and}} V\Sigma^* Z \right)}. \tag{3}$$

DMD with optimal amplitude from Eq. (3) approximates the underling dynamics as a linear evolution form in Eq. (1) or in matrix form in Eq. (2). We refer the triplet $\{(s_k, \phi_k, \alpha_k)\}_{k=1}^r$ as the *DMD triple*. More details on numerical calculation of the DMD can refer to literature[22,28].

Delay embedding

Delay embedding[29] is commonly used for low dimensional time series reconstruction. For a time series $X = (x_t, x_{t+1}, \ldots, x_{t+m-1})$ where x_i is a low dimensional vector in $\mathbb{R}^k$, applying a delay-embedding of embedding time τ gives the Hankel matrix

$$
\mathbb{X} = \begin{bmatrix} x_t & x_{t+1} & \cdots & x_{t+m-\tau} \\ x_{t+1} & x_{t+2} & \cdots & x_{t+m-\tau+1} \\ \cdots & \cdots & \ddots & \cdots \\ x_{t+\tau-1} & x_{t+\tau} & \cdots & x_{t+m-1} \end{bmatrix} \tag{4}
$$

The first and the last $m - \tau$ columns of $\mathbb{X}$ are treated as two matrices $X_{0,1}$ respectively when applying the above DMD.

Results

Time series reconstruction and prediction

In this manuscript, we use the published 3-D acceleration data[30]. In this section, we examine the DMD and the optimal delay embedding time for time series reconstruction. We compare the reconstruction performance with traditional methods using principal component analysis (PCA) and independent component analysis (ICA).

The vertical direction has been reported to have the highest variance and has been used successfully for prediction and classification in 3D coordinate systems measuring the force and moment during freezing of gait events[31]. Figure 1 shows an example of the temporal evolution of vertical acceleration at the ankle. By principal component analysis (PCA), similarly, we find that the vertical and forward ankle accelerations are the principal components. Reconstruction errors for the acceleration data using PCA and ICA are shown in Fig. 2a.

To better reconstruct the data, we apply DMD in conjunction with time delay embedding. We enrich measurements x_t with time-shifted copies of itself, which are also known as delay coordinates. From Fig. 2b we find using a delay embedding time $\tau = RL/10$ (i.e., one 10th of the reconstruction length RL) is optimal for data reconstruction. Moreover, in conjunction with the optimal delay embedding time, DMD using only the vertical ankle acceleration data shows better performance in data reconstruction compared to PCA and ICA, as shown in Fig. 2a.

Next, we test whether using all the 9-dimensional data can enhance the performance in data reconstruction. Figure 3a shows that the DMD using all 9-dimensional data outperforms the reconstruction using only the vertical ankle acceleration coordinate. In the following, we use all 9-dimensional data for DMD calculations.

We further test whether the DMD can accurately predict the time series for the near future. We show in Fig. 4 an example of DMD prediction and in Fig. 3b the error of the predicted time series for 100 steps forwards compared to the original data.

So far, the DMD with optimal delay embedding can reconstruct and predict acceleration signals. In the following section, we use the DMD triple to analyze normal and abnormal gaits.

DMD triple of (ab)normal gaits

When segments of acceleration data are accurately reconstructed and predicted by DMD with small errors, the local time evolution can be effectively approximated and analyzed using the linear system derived from
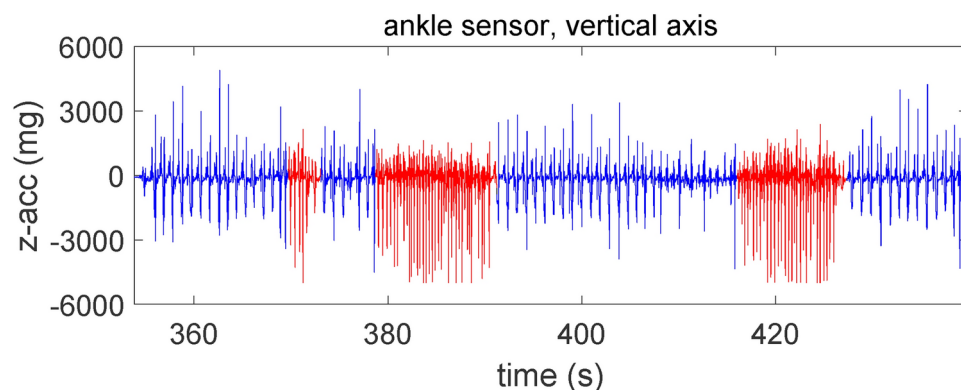

Figure 1. Illustration of the vertical accelerations at ankle (other accelerations at different position/direction are not shown). Normal gait is shown in blue while freezing is shown in red. Note that data are shifted to have a mean of zero.
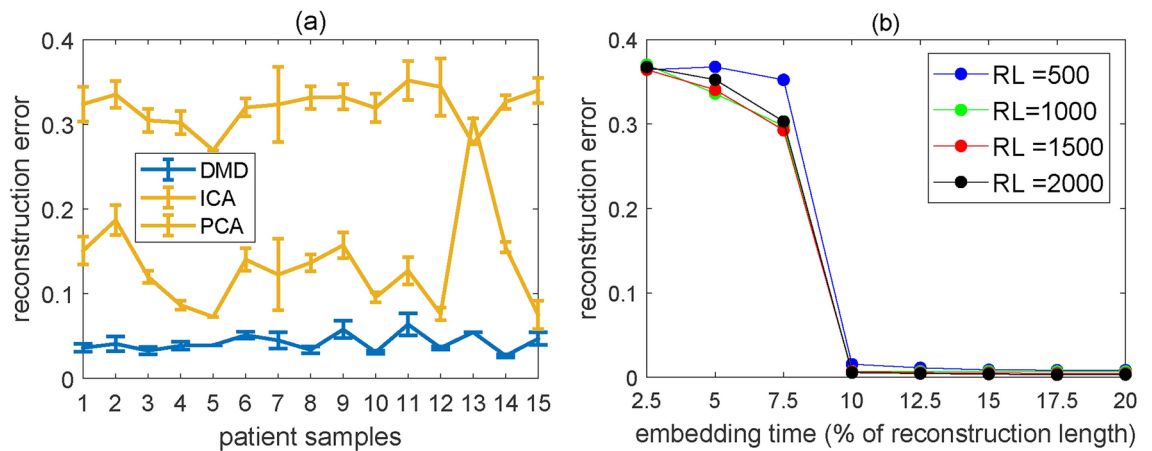
Figure 2. **a** Reconstruction error (mean±sem) $RecErr^{(2)}(X)$ of each patient using DMD, ICA, and PCA respectively. **b** Mean reconstruction error $RecErr^{(2)}(X)$ in association with different embedding times. Reconstruction length (RL) is indicated for each curve. The second component is used for error calculation (see Materials and Methods for details).
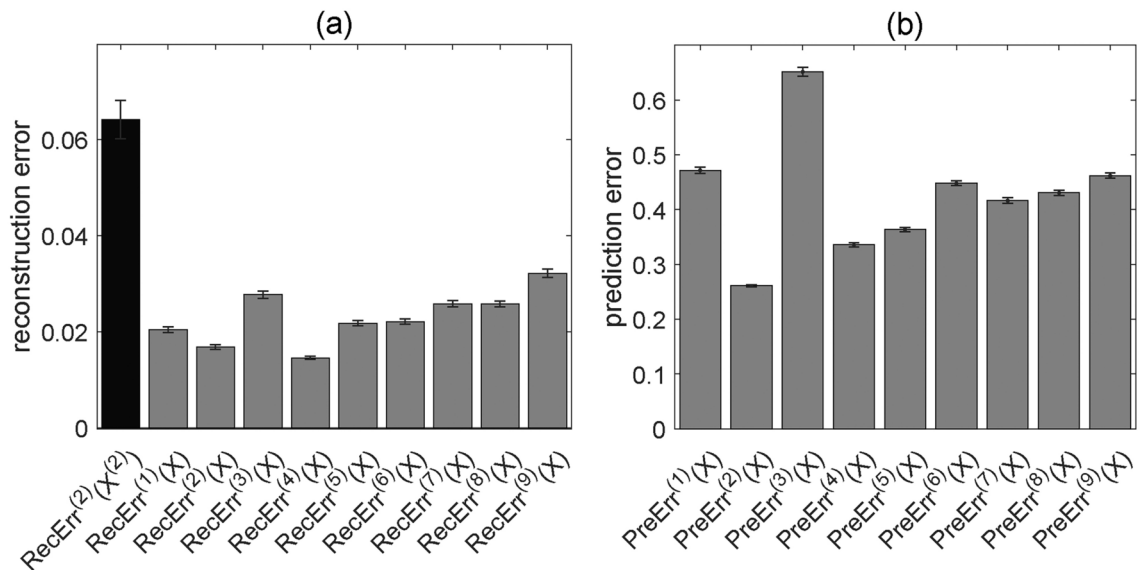

Figure 3. **a** The reconstruction error between real data and data approximated from DMD using the single component $X^{(2)}$ (the ankle vertical direction, black bar) or 9 components X (grey bars). Each grey bar shows the error $RecErr^{(i)}(X)$ computed for each $i-$th component from DMD reconstruction using all 9 components as input. **b** The prediction error $PreErr^{(i)}(X)$ between real data and predicted data from DMD using all 9 components as input. Each grey bar shows the error for each $i-$th component comparison.

the DMD triple. In this section, we compare the DMD triple $\{(s_k, \phi_k, \alpha_k)\}$ between normal and abnormal segments that are well approximated by DMD.

Figure 5 shows one example of the DMD triple. Each value in the amplitude vector reflects the contribution of the corresponding mode throughout the entire time series. A larger amplitude indicates a more pronounced impact of that mode on the system's behavior. From Fig. 5a, we see that normal gaits have relatively larger amplitude, in particular the maximum of the amplitude. Moreover, there are relatively few large amplitudes for both normal and abnormal gaits, suggesting that the system dynamics can be approximated via a few important modes. Thus, we consider the maximal amplitude $a = \max_j\{|a_j|\}$ as an indicator of the overall characteristics of the amplitude. Statistically, over all segments considered, normal gaits have significantly larger maximal amplitude a than abnormal gaits have (t-test, $p < 0.05$)). Figure 5b shows the L^∞ norm of each mode in one DMD triple. It is noticeable that the mode norm is relatively stable for both normal and abnormal gaits and overall the mode norm in normal gaits is slightly larger than that in abnormal gaits. We consider the average of the mode norms $m = \frac{1}{n}\sum_{j=1}^n \|\phi_j\|_\infty$ as an indicator for overall mode norms. Figure 5c shows that the
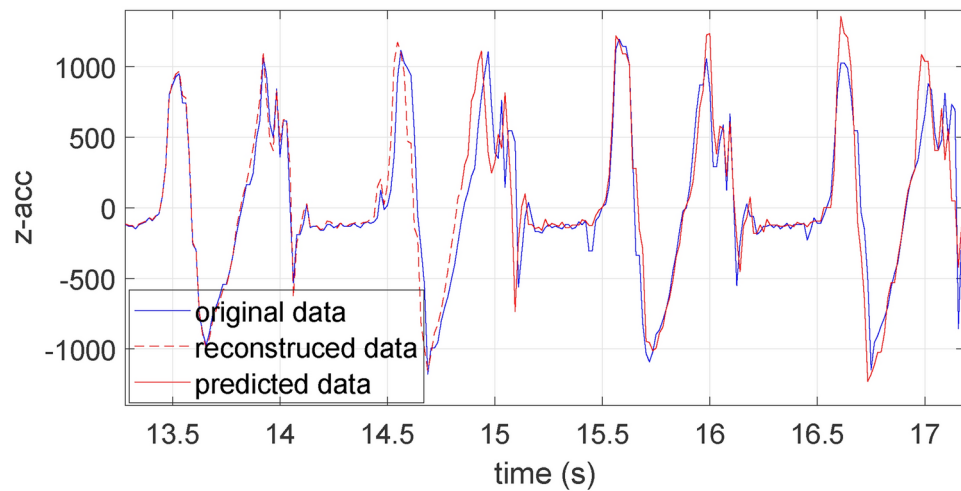
Figure 4. Illustration of the time series reconstructed (dashed line) and predicted (solid red line) from DMD calculations. The first 13 s are excluded in the plot for visualization effect.
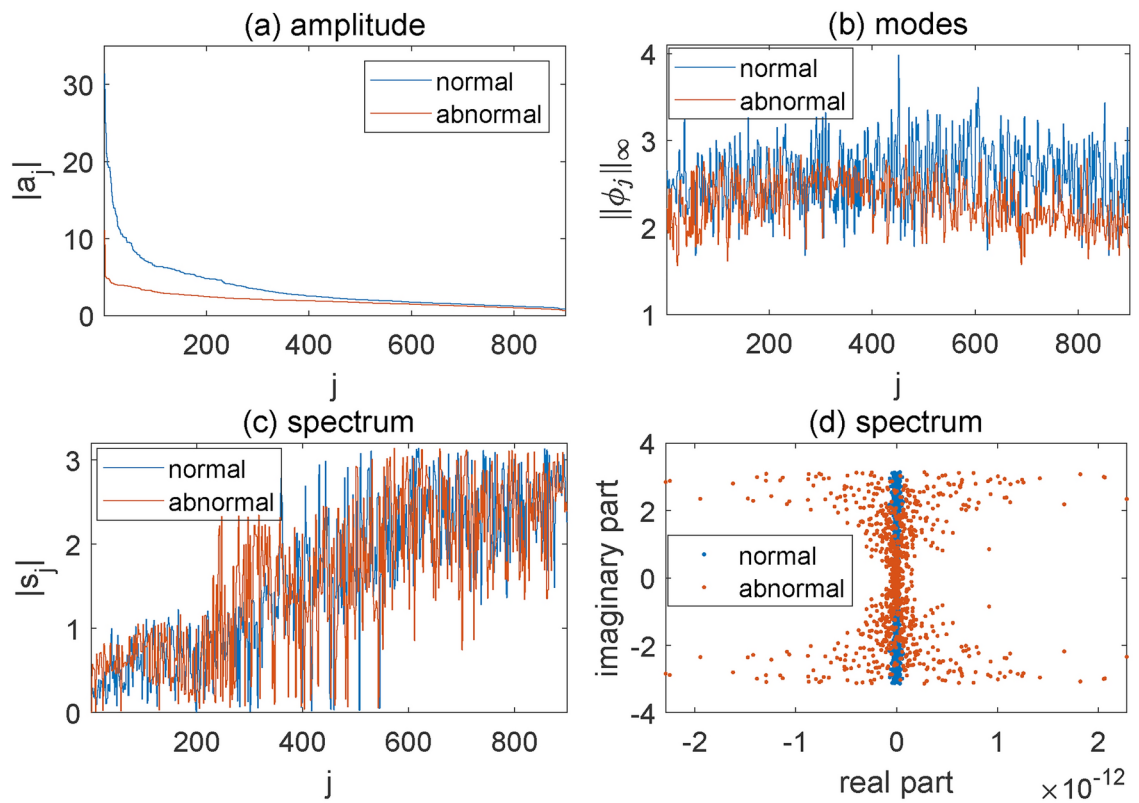

Figure 5. Illustration of DMD triple for one normal and one abnormal gait. **a** All the amplitudes a_j in a descending order. **b** The L^∞ norm for each mode vector ϕ_j. **c** All the norms of spectra s_j while **d** The spectra in the complex plane. Note that the real parts of the spectra for both normal and abnormal gaits are close to zero. We remark here that modes and spectra are reordered according to amplitudes. Note that complex values of DMD triple may occur in the numerical calculation, norm of complex values are used in the plots.

spectrum between normal and abnormal gaits is not very distinct. Furthermore, from Fig. 5d, both normal and abnormal gaits have almost zero in the real part of the spectrum and the imaginary part spans over a similar range.

The dynamics for (ab)normal states among different patients could be different, and we consider all selected segments for individual patients for analysis. Figure 6a, b show the overall mode norm m and the amplitude
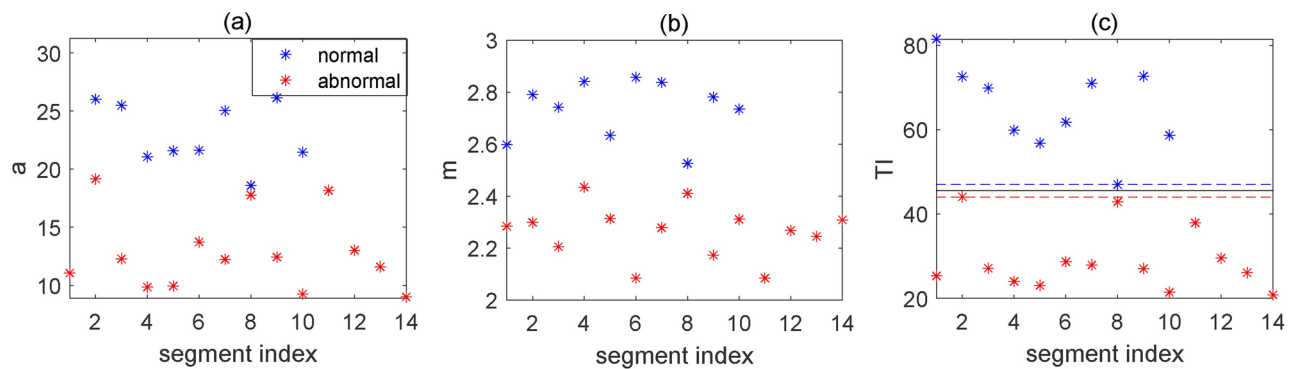
Figure 6. Illustrations of triple index and threshold identification in one patient. **a** The maximal amplitude $a = \max_j \{|a_j|\}$ for both normal and abnormal gaits. **b** The average of mode norms $m = \frac{1}{n} \sum_j \|\phi_j\|_\infty$. **c** The triple index $TI = ma$ with a threshold (solid black line) identified via SVM and the corresponding upper and lower margins (blue and red dashed lines).

indicator a for all segments considered in one patient. Consistent with Fig. 5, normal gaits have a higher overall maximal amplitude and an overall mode norm compared to abnormal gaits. To distinguish between normal and abnormal gaits using the DMD triple, we introduce a *triple index* calculated as $TI = ma$ (see Materials and Methods). From Fig. 6c, we can see that normal gaits have a relatively larger TI than abnormal gaits for the same patient, and the triple indexes between normal and abnormal gaits are well separated by a threshold obtained using the support vector machine (SVM) method[32]. Thus, we have patient-specific thresholds of *TI* separating normal and abnormal gaits for individual patients.

Classification and prediction of FoG

In this section, we test the patient-specific thresholds obtained above to predict and classify FoG for all individual patients.

We use long continuous time-series segments that encompass at least 150 data points of normal data (which are necessary to appropriately compute the DMD triple for normal gaits), followed by abnormal data. We calculate the time evolution of the triple index using a moving window of 25 step size and a fixed reconstruction length of 150 step size; see Fig. 7 for two examples. Once the triple index is lower than the threshold obtained for the patient, we consider that gait freezing occurs. The triple index may fluctuate around the threshold. To better identify the freezing of gait from the changes of triple index over time, we consider that freezing is predicted in advance if the triple index at the actual medically identified transition time is smaller than the corresponding threshold (the specific gap is at least 0.5). We further calculate the time interval from the actual transition time to its closest time when the triple-index curve intersects with the threshold. Using this approach, among all potential segments, we can predict FoG early on for 81.97% of all possible segments, with an average early prediction time 6.13 ± 0.82 s ($n = 50$). This early prediction time is better than the published 1–5 s[33–37]; see Table 1. We observe that, in certain instances, our predicted freezing time may slightly lag behind the actual transition time. However, those delay prediction times (1.03 ± 0.26 s ($n = 11$)) are small.

For the classification performance using the triple index, we calculate the proportion of time points where the relationship between the triple index and the threshold line matches the classification in the original data, i.e., higher than the threshold is identified as normal while lower than the threshold is identified as abnormal (freezing). Our approach gives FoG classification accuracy of 86.5%, sensitivity of 88.1%, and specificity of 87.9%. This is comparable to the performance reported, though not better than the best performance reported; see Table 1.

Considering that patients may interrupt their movements during experiments, identifying FoG from these stopping events can also be beneficial. Our proposed DMD triple index can identify FoG from stopping events if an appropriate threshold can be obtained. For example, in one patient (Fig. 8a, b) with all possible time segments analyzed, we achieved classification with 67.2% accuracy, 76.6% sensitivity, and 58.4% specificity. However, the triple indexes can be similar between FoG and stopping events; see Fig. 8c. In this case, the triple index fails to identity FoG from stopping events; see Fig. 8d for example.

Materials and methods
Dataset description

The acceleration FoG dataset used in this manuscript was published previously[30]. 3D acceleration data were captured by three wearable wireless acceleration sensors positioned on the ankle, thigh, and hip at 64 Hz of patients with a history of FoG. Patients were tested in the morning during the OFF stage of the medication cycle and asked to perform basic walking tasks designed to represent different aspects of daily walking.
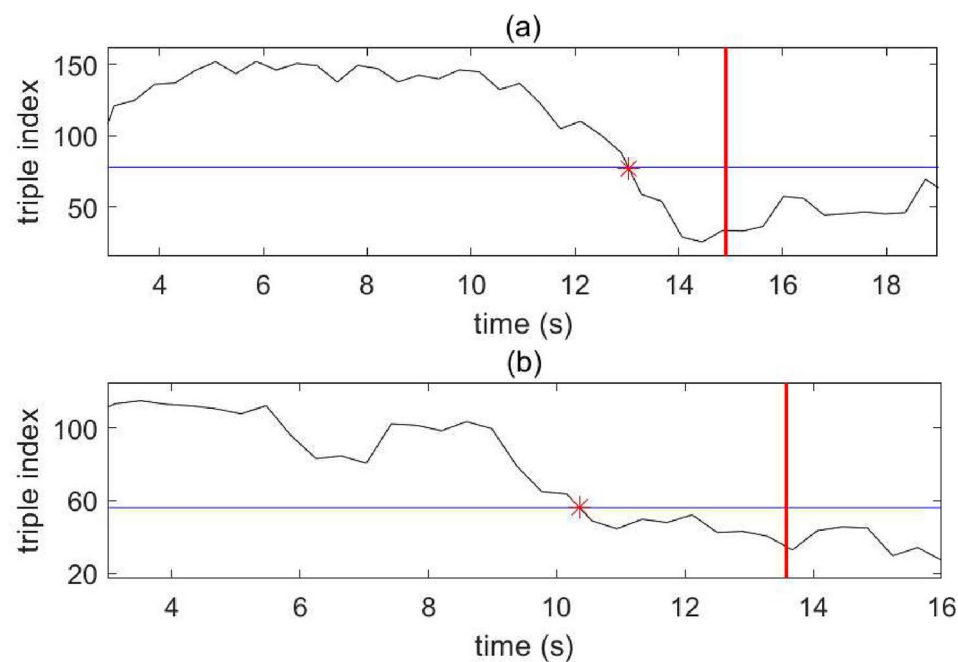
Figure 7. The time evolution of triple index used to predict FoG in two patients. The red star indicates the predicted transition time to freeze and its time distance to the red lines (the transition time from normal to abnormal gait in the original data) gives the early prediction time. The blue line indicates the triple index threshold obtained between normal and abnormal gaits.

Method	Features	Early prediction time (%)	Accuracy (%)	Sensitivity (%)	Specificity (%)
LSTM network[33]	Raw data	1–5	79.5–87.5	N/A	N/A
Ensemble classifiers	Freeze index; entropy;				
with ADASYN[34]	Power; standard deviation	0–2	N/A	90.8	95
AdaBoost[35]	Impaired gait features;				
	Conventional FoG				
	Detection features	0.93	82.7	N/A	N/A
RF, XGB, GMB[36]	RMS velocity; entropy;				
RBF-SVM, MLP	Freeze index; FFT phase	2–4	N/A	72.3	87.4
DMD, triple index	Raw data	6.13	86.5	88.1	87.9

Table 1. Comparison of performance with other methods reported using the same original dataset[30]. Note that the values from other methods are sourced from corresponding original papers.

Preprocess of the data

For a time series segment, its time average is subtracted before applying a delay-embedding dynamic mode decomposition. More precisely, suppose a time series $X = (x_0, x_1, \ldots, x_{n-1})$ of n data points, where each data point $x_i \in \mathbb{R}^k$ is a $k-$dimensional vector. We adjust it by subtracting its time average and denote the adjusted time series as $X' = (x'_0, x'_1, \cdots, x'_{n-1})$ where $x'_j = x_j - \frac{1}{n} \sum_{i=0}^{n-1} x_i$.

ICA and PCA reconstruction

ICA reconstruction of acceleration data is performed using the fastica algorithm[38] with three components of the largest weight norm, while the PCA reconstruction method is performed using the three most significant principal components.

DMD reconstruction and prediction

We combine delay embedding with DMD. More precisely, we use the Hankel matrix $\mathbb{X}$ in Eq. (4) as an input to calculate the DMD triple $\{(s_k, \phi_k, \alpha_k)\}_{k=1}^r$ and then use Eq. (2) to calculate the time evolution of signals $\tilde{x}_t$ as
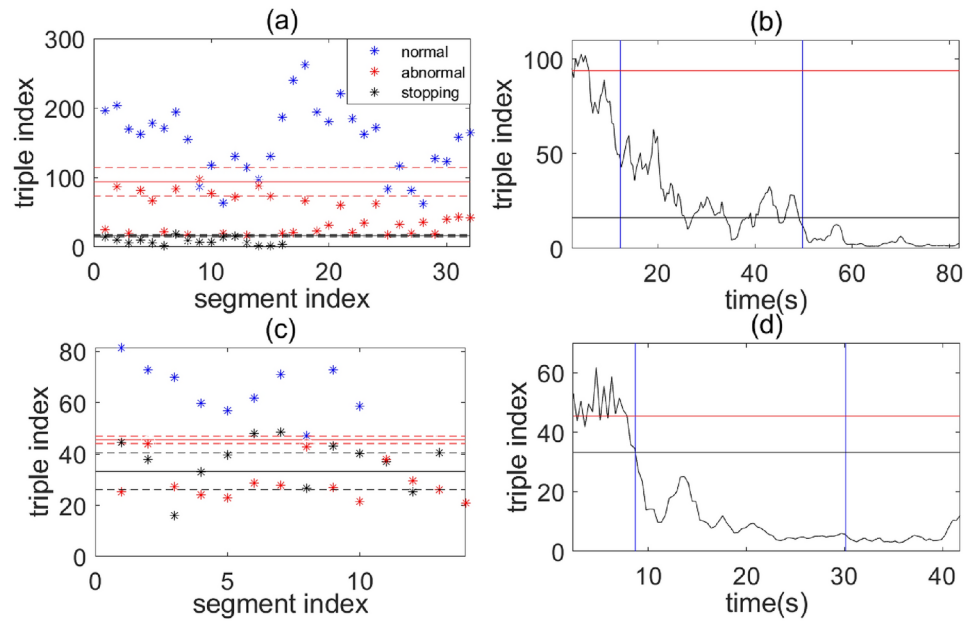
Figure 8. **a** and **c** The triple index with thresholds (red and black solid lines) and corresponding upper and lower margins (dashed lines) identified via SVM between normal and abnormal gaits as well as between abnormal and stopping events in two patients respectively. **b** and **d** show the time evolution of the triple index with thresholds (red and blue lines) obtained from (**a**) and (**c**) for two patients respectively. Blue vertical lines are the transition times in the original data.

$$
\begin{bmatrix}
\tilde{x}_0 & \tilde{x}_1 & \cdots & \tilde{x}_{n-\tau} \\
\tilde{x}_1 & \tilde{x}_2 & \cdots & \tilde{x}_{n-\tau+1} \\
\cdots & \cdots & \ddots & \cdots \\
\tilde{x}_{\tau-1} & \tilde{x}_\tau & \cdots & \tilde{x}_{n-1}
\end{bmatrix}
= [\phi_1, \ \phi_2, \cdots \phi_r]
\begin{bmatrix}
\alpha_1 & 0 & \cdots & 0 \\
0 & \alpha_2 & \cdots & 0 \\
\vdots & \vdots & \ddots & \vdots \\
0 & 0 & \cdots & \alpha_r
\end{bmatrix}
\begin{bmatrix}
1 & e^{s_1} & \cdots & e^{s_1(n-\tau-1)} \\
1 & e^{s_2} & \cdots & e^{s_2(n-\tau-1)} \\
\vdots & \vdots & \ddots & \vdots \\
1 & e^{s_r} & \cdots & e^{s_r(n-\tau-1)}
\end{bmatrix}
\tag{5}
$$

We calculate the average of $\tilde{x}_t$ from the above matrix with the same subscription along the antidiagonal and denote its average as $\hat{x}_t$ as the eventual predicted signal at time t.

Error calculation

The error of the eventual output time evolution $\hat{X} = [\hat{x}_0, \hat{x}_1, \hat{x}_2, \ldots, \hat{x}_{n-1}]$ from DMD compared with the original data $X' = (x'_0, x'_1, \cdots x'_{n-1})$ (with mean subtracted) for each component i is calculated as

$$
error^{(i)}(X', \hat{X}) = \frac{MAE(X'^{(i)}, \hat{X}^{(i)})}{|X'^{(i)}_{0.85} - X'^{(i)}_{0.15}|}
$$

where $X'^{(i)}$ represents the i-th row of matrix X', $X'^{(i)}_{0.85}$ and $X'^{(i)}_{0.15}$ refers to the 85th and 15th percentiles of its i-th row. Here $MAE(X'^{(i)}, \hat{X}^{(i)})$ refers to the mean absolute error. Note that the maximal/minimal signals between different data segments could be largely different, we thus use 85th and 15th percentiles instead of maximum and minimum.

We refer to the error of the reconstructed time series as reconstruction error, denoted as $RecErr^{(i)}(X) = error^{(i)}(X', X_{rec})$ where $X_{rec} = [\hat{x}_0, \hat{x}_1, \hat{x}_2, \ldots, \hat{x}_n]$. Also we refer to the error of predicted time series as the prediction error, denoted as $PreErr^{(i)}(X) = error^{(i)}(X', X_{pre})$ where $X_{pre} = [\hat{x}_{n+1}, \ldots, \hat{x}_m]$. In the manuscript, the error $error^{(2)}$ is mostly used, and we omit the superscript without any ambiguity. We would like to remark that when referring to a single vector component, say $i-$th component, we denote the corresponding reconstruction and prediction errors as $RecErr^{(i)}(X^{(i)})$ and $PreErr^{(i)}(X^{(i)})$.

Triple index

DMD-based approach outputs the DMD triple $\{s_k, \phi_k, \alpha_k\}$. We define $m = \frac{1}{n}\sum_{k=1}^{n} \|\phi_k\|_\infty$ where $\|\cdot\|_\infty$ refers to the infinity norm and is calculated as the maximum absolute value of its components and

$a = \max\{|a_1|, |a_2|, \ldots, |a_n|\}$. We then define *triple index* $TI(x) = m \cdot a$. The threshold of triple index differentiating normal and abnormal gaits is obtained by SVM with a linear kernel function.

To appropriately analyze the triple index between normal and abnormal gaits, we choose time series segments with reconstruction and prediction length that are best captured by DMD. More precisely, we split the long time series into segments of length L and use the first part of each segment (at least 200 data points) to calculate the DMD and the last n data points of the segment for DMD prediction. We calculate the prediction error for various L from $300, 400, \cdots$, up to 2000 and various n from 100 to 500. Note that there are only a small number of abnormal events. In order to obtain reasonable comparable statistics of the DMD triple index between normal and abnormal segments, we choose a similar amount of normal and abnormal segments with small prediction errors. More precisely, the normal segments we selected have prediction errors less than 0.09 while the abnormal ones have prediction errors less than 1.47.

The above process is also used to identify FoG from stopping events in one patient where the triple index can be appropriately obtained through SVM. The time series segments of stopping state we selected have prediction errors less than 0.86 while the abnormal gaits have prediction errors less than 1.47.

Conclusion and discussion

Using DMD together with an optimal delay embedding time, we explore the gait acceleration dynamics underlying time series from patients with FoG. We identified that normal and abnormal gaits differ significantly in amplitudes whereas their spectra are similar. Based on this, we introduce a *triple index* $TI = ma$, i.e., the multiplication of the maximal amplitude a and the average of mode norms m. By statistical analysis of the triple index between normal and abnormal gaits, we obtained individual threshold values for each patient. Using these patient-specific thresholds, we successfully classified FoG with an accuracy of 86.5%, a sensitivity of 88.1%, and a specificity of 87.9%. Additionally, we can predict the onsets of FoG events within 6.13 s on average in advance. This prediction time in advance is better than the published early prediction time 1–5 s[33–37].

In the *triple index* $TI = ma$, a high value of m may indicate that energy is highly concentrated in certain modalities rather than evenly distributed across modalities. This may be due to some specific physiological or pathological conditions. Also, a high amplitude a indicates the presence of dominant modes with corresponding amplitude, which might be associated with the coordination and stability of a healthy gait. In contrast, a low amplitude a in pathological gait might be related to motor impairments leading to gait disharmony and dynamic imbalance, affecting the smoothness and efficiency of walking. Taking together, $TI = ma$ somehow relates to the maximal signal among the time evolution, which has been considered as one of the features in machine learning methods[39]. Here using the DMD approach, we simply use TI to identify FoG without referring to other features.

Moreover, this DMD-based approach has the potential to be applied to real-time patient-specific FoG prediction during movement. Once an appropriate threshold of the triple index is identified, one can classify and predict FoG from the evolution of the triple index using a moving window. In this manuscript, a moving window with 0.4 s moving speed was used. A finer moving window could be used to refine the FoG onset time prediction, though this could be computationally heavy.

Identifying FoG from stopping events might also be useful. However, the current triple index based on DMD would fail to identify FoG if the triple indexes are statistically similar between FoG and stopping events. Then, constructions of more complex indexes or features from DMD triplets are necessary to improve the identification of FoG.

Another improvement on this DMD-based approach for real-time application could involve the identification of optimal amount of time series segments required to obtain reliable triple index threshold. Such optimization problem is also critical in machine learning and deep learning methods[40].

Data availability

The raw freezing of gait data is published previously[30] and is publicly available at the Daphnet Freezing of Gait Dataset https://archive.ics.uci.edu/dataset/245/daphnet+freezing+of+gait.

References
1. Braak, H., Ghebremedhin, E., Rüb, U., Bratzke, H. & Del Tredici, K. Stages in the development of Parkinson's disease-related pathology. *Cell Tissue Res.* **318**, 121–134 (2004).
2. Macht, M. et al. Predictors of freezing in Parkinson's disease: a survey of 6620 patients. *Mov. Disord.* **22**, 953–956 (2007).
3. Schaafsma, J. et al. Characterization of freezing of gait subtypes and the response of each to levodopa in Parkinson's disease. *Eur. J. Neurol.* **10**, 391–398 (2003).
4. Schaafsma, J. et al. Characterization of freezing of gait subtypes and the response of each to levodopa in Parkinson's disease. *Eur. J. Neurol.* **10**, 391–398 (2003).
5. Okuma, Y., Silva de Lima, A., Fukae, J., Bloem, B. & Snijders, A. A prospective study of falls in relation to freezing of gait and response fluctuations in Parkinson's disease. *Parkinsonism Relat. Disord.* **46**, 30–35 (2018).
6. Ward-Griffin, C. et al. Falls and fear of falling among community-dwelling seniors: the dynamic tension between exercising precaution and striving for independence. *Can. J. Aging* **23**, 307–318 (2004).
7. Zhang, W. et al. Detection and prediction of freezing of gait with wearable sensors in Parkinson's disease. *Neurol. Sci.* **45**, 431–453 (2024).
8. Nieuwboer, A. et al. Electromyographic profiles of gait prior to onset of freezing episodes in patients with Parkinson's disease. *Brain* **127**, 1650–60 (2004).
9. Pardoel, S., Kofman, J., Nantel, J. & Lemaire, E. Wearable-sensor-based detection and prediction of freezing of gait in Parkinson's disease: a review. *Sensors (Basel)* **19**, 1–37 (2019).

10. di Biase, L., Pecoraro, P., Pecoraro, G., Shah, S. & di Lazzaro, V. Machine learning and wearable sensors for automated Parkinson's disease diagnosis aid: a systematic review. *J. Neurol.* (2024).

11. Sun, H., Ye, Q. & Xia, Y. Predicting freezing of gait in patients with Parkinson's disease by combination of manually-selected and deep learning features. *Biomed. Signal Process. Control* **88**, 105639 (2024).

12. Kleanthous, N., Hussain, A., Khan, W. & Liatsis, P. A new machine learning based approach to predict freezing of gait. *Pattern Recognit. Lett.* **140**, 119–126 (2020).

13. Arami, A., Poulakakis-Daktylidis, A., Tai, Y. & Burdet, E. Prediction of gait freezing in Parkinsonian patients: a binary classification augmented with time series prediction. *IEEE Trans. Neural Syst. Rehabil. Eng.* **27**, 1909–1919 (2019).

14. Palmerini, L. et al. Identification of characteristic motor patterns preceding freezing of gait in Parkinson's disease using wearable sensors. *Front. Neurol.* **8**, 394 (2017).

15. Xia, Y., Sun, H., Zhang, B., Xu, Y. & Ye, Q. Prediction of freezing of gait based on self-supervised pretraining via contrastive learning. *Biomed. Signal Process. Control* **89**, 105765 (2024).

16. Mohammadian Rad, N., Van Laarhoven, T., Furlanello, C. & Marchiori, E. Novelty detection using deep normative modeling for IMU-based abnormal movement monitoring in Parkinson's disease and autism spectrum disorders. *Sensors (Basel)* **18**, 3533 (2018).

17. Borzì, L. et al. Prediction of freezing of gait in Parkinson's disease using wearables and machine learning. *Sensors (Basel)* **21**, 614 (2021).

18. Pham, T. et al. Freezing of gait detection in Parkinson's disease: a subject-independent detector using anomaly scores. *IEEE Trans. Biomed. Eng.* **64**, 2719–2728 (2017).

19. Parakkal Unni, M. et al. Data-driven prediction of freezing of gait events from stepping data. *Front. Med. Technol.* **2**, 581264 (2020).

20. Cenedese, M., Axås, J., Bäuerlein, B., Avila, K. & Haller, G. Data-driven modeling and prediction of non-linearizable dynamics via spectral submanifolds. *Nat. Commun.* **13**, 872 (2022).

21. Mauroy, A., Susuki, Y. & Mezić, I. Introduction to the Koopman operator in dynamical systems and control theory. In: *The Koopman Operator in Systems and Control*, Lecture Notes in Control and Information Sciences, 3–33 (Springer, 2020).

22. Tu, J., Rowley, C., Luchtenburg, D., Brunton, S. & Kutz, J. On dynamic mode decomposition: theory and applications. *J. Comput. Dyn.* **1**, 391–421 (2014).

23. Kutz, J., Brunton, S., Brunton, B., Proctor, J. Chapter 1: Dynamic mode decomposition: an introduction. In *Dynamic Mode Decomposition*, 1–24 (SIAM, Philadelphia, PA, 2016).

24. Schmid, P., Li, L., Juniper, M. & Pust, O. Applications of the dynamic mode decomposition. *Theor. Comput. Fluid Dyn.* **25**, 249–259 (2011).

25. Fernández, O., Iqbal, M. & Gusrialdi, A. An improved dynamic mode decomposition for real-time electromechanical oscillation monitoring in power systems: the impact of ultra-low frequency modes and its removal strategy. *IET Gener. Transm. Dis.* **17**, 4574–4591 (2023).

26. Liew, J., Göçmen, T., Lio, W. & Larsen, G. Streaming dynamic mode decomposition for short-term forecasting in wind farms. *Wind Energy* **25**, 719–734 (2022).

27. Mezić, I. et al. A Koopman operator-based prediction algorithm and its application to Covid-19 pandemic and influenza cases. *Sci. Rep.* **14**, 1–13 (2024).

28. Jovanović, M., Schmid, P. & Nichols, J. Sparsity-promoting dynamic mode decomposition. *Phys. Fluids (1994)* **26**, 024103 (2014).

29. Kennel, M., Brown, R. & Abarbanel, H. Determining embedding dimension for phase-space reconstruction using a geometrical construction. *Phys. Rev. A* **45**, 3403–3411 (1992).

30. Bächlin, M. et al. Wearable assistant for Parkinsons disease patients with the freezing of gait symptom. *IEEE Trans. Inf. Technol. Biomed.* **14**, 436–446 (2010).

31. Parakkal Unni, M. et al. Data-driven prediction of freezing of gait events from stepping data. *Front. Med. Technol.* **2**, 581264 (2020).

32. Apsemidis, A. & Psarakis, S. A review and applications in statistical process monitoring, *Support Vector Mach.* (2020).

33. Torvi, V. G., Bhattacharya, A. & Chakraborty, S. Deep domain adaptation to predict freezing of gait in patients with Parkinson's disease. In *2018 17th IEEE International Conference on Machine Learning and Applications (ICMLA)* (IEEE, 2018).

34. Naghavi, N., Miller, A. & Wade, E. Towards real-time prediction of freezing of gait in patients with Parkinson's disease: addressing the class imbalance problem. *Sensors (Basel)* **19**, 3898 (2019).

35. Zhang, Y. et al. Prediction of freezing of gait in patients with Parkinson's disease by identifying impaired gait patterns. *IEEE Trans. Neural Syst. Rehabil. Eng.* **28**, 591–600 (2020).

36. Kleanthous, N., Hussain, A. J., Khan, W. & Liatsis, P. A new machine learning based approach to predict freezing of gait. *Pattern Recognit. Lett.* **140**, 119–126 (2020).

37. Ouyang, S., Chen, Z., Chen, S. & Zhao, J. Prediction of freezing of gait in Parkinson's disease using time-series data from wearable sensors. In *2023 42nd Chinese Control Conference (CCC)* (IEEE, 2023).

38. Hyvarinen, A. Fast and robust fixed-point algorithms for independent component analysis. *IEEE Trans. Neural Netw.* **10**, 626–634 (1999).

39. Kaviya, B., Prasanna, J., Nancy, R., Subathra & George S. T. Maximum overlap discrete wavelet packet transform-based feature extraction for recognition of freezing of gait in parkinson's disease using gait signals. In *International Conference on Computer Vision and Internet of Things 2023 (ICCVIoT'23)*, 120–126 (IET, 2023).

40. Goschenhofer, J. *et al.* Wearable-based Parkinson's disease severity monitoring using deep learning. In *Machine Learning and Knowledge Discovery in Databases*, Lecture Notes in Computer Science, 400–415 (Springer, Cham, 2020).

Acknowledgements

Author contributions

Z.F. performed the analysis and edited the manuscript, C.L. and Y.Z. conceived and designed the project and edited the manuscript. All authors reviewed the manuscript.

Declarations

Competing interests
The authors declare no competing interests.

Additional information
Correspondence and requests for materials should be addressed to Y.Z.

Reprints and permissions information is available at www.nature.com/reprints.

Publisher's note Springer Nature remains neutral with regard to jurisdictional claims in published maps and institutional affiliations.